Abstract

Hierarchical three-dimensional (3D) porous architecture $Fe^{II}Fe^{III}$ and $Co^{II}Fe^{III}$ layered double hydroxide (LDH) multiwall were grown on carbon-felt (CF) substrate via solvothermal process. The as-deposited $Fe^{II}Fe^{III}$ and $Co^{II}Fe^{III}$ LDH/CF cathodes were composed of highly oriented and well crystallized interconnected nanowalls with high electrical conductivity and excellent catalytic activity over a wide pH range (pH 3 – 9) for heterogeneous electro-Fenton (HEF) degradation of antibiotic sulfamethoxazole (SMT) in aqueous medium. Mineralization efficiencies (in terms of TOC removal) of ~97%, 93% and 90% was achieved at pH 3, 6 and 9 respectively for both $Fe^{II}Fe^{III}$ and $Co^{II}Fe^{III}$ LDH/CF cathodes in HEF system at analogous experimental conditions. However, comparative electro-Fenton (EF) with 0.2 mM Fe^{2+} or electrooxidation with H_2O_2 production (EO-H_2O_2) studies using Ti_4O_7 anode at similar experimental conditions showed relatively lower mineralization with highest TOC removal efficiency of 77% and 64% obtained at pH 3 for EF-Fe^{2+} and EO-H_2O_2 respectively. Oxidative degradation of SMT in HEF was by (i) $Ti_4O_7(^{\bullet}OH)$ generated at anode surface at all pH, (ii) surface catalyzed process and (iii) contribution from homogeneous catalyzed process at pH 3 due to leached iron ions. The prepared $Fe^{II}Fe^{III}$ LDH/CF exhibited excellent catalytic stability with good reusability up to 10 cycles of 4 h treatment at pH 6. Initial SMT solution showed relatively high toxicity but total detoxification of the solution was attained after 8 h of treatment by HEF with $Fe^{II}Fe^{III}$ LDH/CF cathode. Both cathodes exhibited similar catalytic efficiency; however the $Fe^{II}Fe^{III}$ LDH/CF was preferred to $Co^{II}Fe^{III}$ LDH/CF since Co is considered toxic.

Keywords: $Fe^{II}Fe^{III}$ and $Co^{II}Fe^{III}$ LDH modified carbon felt, heterogeneous electro-Fenton, catalytic activity, Sulfamethoxazole, mineralization, Microtox® toxicity

1. Introduction

Nowadays, electrochemical advanced oxidation processes (EAOPs) receive increasing attention due to their excellent potential for total destruction of refractory organic pollutants in wastewater [1–4]. These eco-friendly wastewater treatment techniques utilize *in-situ* generated reactive oxygen species, mostly hydroxyl radicals ($^{\bullet}OH$), which is the second strongest oxidizing species after fluorine (E^o ($^{\bullet}OH/H_2O$) = 2.80 V/SHE) and can non-selectively oxidize organic pollutants until their total mineralization (electrochemical combustion) to CO_2, water and inorganic ions [2,5–7]. EAOPs based on Fenton's chemistry (electro-Fenton and related process) are one of the most widely studied techniques among EAOPs for wastewater treatment [2,4]. In electro-Fenton process (EF), $^{\bullet}OH$ are continuously produced *via* the reaction between electrochemically generated Fenton's reagent ($H_2O_2 + Fe^{2+}$) (eq. 1) in the bulk solution [4,6,8]. The required H_2O_2 is continuously electrogenerated *in-situ* by two-electrons reduction of dissolved oxygen at the cathode (eq. 2) and only catalytic quantity of Fe^{2+} is added to catalyze its decomposition because Fe^{2+} is continuously regenerated from the Fe^{3+} formed in Fenton's reaction (eq.1) by electro-reduction at the cathode (eq. 3) [2,4,9].

$$Fe^{2+} + H_2O_2 \rightarrow Fe^{3+} + H_2O + {}^{\bullet}OH \quad (1)$$

$$O_2 + 2H^{+} + 2e^{-} \rightarrow H_2O_2 \quad (2)$$

$$Fe^{3+} + e^{-} \rightarrow Fe^{2+} \quad (3)$$

However, some major challenges are commonly encountered when using homogeneous EF process. For instance homogeneous EF is only optimal at very narrow pH window (pH 2.5 – 3.5), as such working outside this pH drastically reduces the efficiency of the process [10–13]. This is not beneficial when treating real industrial effluents/wastewater, which usually have divergent pH depending on the origin. Further, the catalyst in homogeneous EF has limited recyclability and reusability and effluent must be neutralized before disposal to nullify the acidic condition, which may also results in generation of sludge that may require a secondary process for its disposal [10,12].

HEF process has been developed to overcome these challenges since it is effective over a wide pH range, including basic pH, with the reusability and recyclability of the solid catalyst

[12]. Also, the need for post-treatment neutralization and formation of iron-rich sludge encounter in homogeneous EF system is completely eliminated with the use of heterogeneous catalyst. Based on literature, heterogeneous catalysts such as natural Fe minerals [14–18], supported transition metal/metal oxides [10,19–24] and Ferrite, Fe-CuC and Fe-Co – carbon aerogel [12,25–27] have been investigated for degradation of the various class of organic pollutants. Excellent mineralization of organics as a result of both homogeneous and surface catalyzed process has been reported for ferrite, pyrite, goethite and magnetite as heterogeneous catalysts in HEF especially at acid pH, however such system demonstrated low recyclability and reusability. Fe/Fe-oxides supported on activated carbon or clay materials have been reported to show high adsorption property for some pollutants which hinders and delays the catalytic activities of the heterogeneous catalysts [28]. Although studies have shown that carbon aerogel containing ferrite, magnetite, Fe-CuC or Fe-CoC exhibited high catalytic activity and reusability over wide pH range; the synthesis route seems complex for large scale production [25,26]. Recently we reported excellent performance of CoFe-layered double hydroxide (LDH) modified carbon-felt cathode for mineralization of acid-orange II [13] but the use of Cu and Co in either carbon aerogel or LDH modified cathode is dangerous because both are considered toxic. In fact, leaching of Co or Cu at acidic and neutral pH has been reported for aerogel and LDH applied in HEF process [13,25,26,29].

SMT is one of the most widely used sulfonamide antibiotics against aerobic bacteria and protozoa and its combination with other antibiotics is largely administered for the treatment of respiratory disease like pneumonia [30,31]. Several studies have reported the occurrence of SMT at different concentration levels (ng L^{-1} to μg L^{-1}) in various municipal sewage treatment plants (STPs), surface water, hospital effluents, animal impoundments and even drinking water [32]. Similar to other pharmaceuticals, the presence of SMT has become a serious environmental concern due to its continuous accumulation and resistance to natural attenuation processes [33]. SMT is refractory to the conventional treatment used in STPs, but many advanced oxidation processes (AOPs) have been applied as an alternative treatment for the degradation of SMT [31]. Among the AOPs, EAOPs such as EO and EF have been reported to achieve excellent decontamination of SMT solution [30,31,33].

In this study, $Fe^{II}Fe^{III}$ and $Co^{II}Fe^{III}$ LDH were grown on CF by solvothermal process. The prepared cathodes were characterized by X-ray diffraction (XRD) measurement, Scanning electron microscopy (SEM), Fourier-transform infrared spectroscopy (FTIR), X-ray photoelectron spectroscopy (XPS) and Electrochemical impedance spectroscopy (EIS) to examine their structural and electrochemical properties. The catalytic activity of the $Fe^{II}Fe^{III}$ and $Co^{II}Fe^{III}$ LDH modified CF cathodes were evaluated by studying the HEF mineralization of SMT at pH 3 – 9. Besides, sub-stoichiometric titanium oxide (Ti_4O_7) was used as the anode material. This electrode has been demonstrated to be efficient in electrochemical wastewater treatment and capable of producing heterogeneous hydroxyl radical ($Ti_4O_7(^{\bullet}OH)$) at it surface via water oxidation (eq. 4) for mineralization of organics, which can contribute to the overall efficiency of the HEF process [34–36].

$$Ti_4O_7 + H_2O \rightarrow Ti_4O_7(^{\bullet}OH) + H^+ + e^- \quad (4)$$

In addition, the evolution of the toxicity of the SMT solution during the HEF treatment was examined using Microtox® method.

2. Materials and methods

2.1 Chemicals

CF was obtained from Alfa Aesar. Iron II sulfate heptahydrate, $FeSO_4.7H_2O$ (> 99% purity); iron III nitrate nonahydrate, $Fe(NO_3)_3.9H_2O$ (98% purity); Cobalt II nitrate tetrahydrate, $Co(NO_3)_2.4H_2O$ (> 99% purity); urea, $CO(NH_2)_2$ and ammonium fluoride, NH_4F (99% purity) were purchased from Sigma Aldrich and used for the synthesis of LDH coating on the CF without further purification. SMT, $C_{10}H_{11}N_3O_3S$ and sodium sulfate, Na_2SO_4 (anhydrous, 99-100%) were also supplied by Sigma Aldrich. Bioluminescent bacteria *Vibrio fischeri* and the activation reagent LCK 487 LUMISTOX used in Microtox® were supplied by Hach Lange France SAS. All solutions were prepared with ultra-pure water obtained from a Millipore Mill-Q system with resistivity > 18 MΩ cm at room temperature. Organic solvents and other chemicals used were either HPLC or analytic grade from Sigma-Aldrich, Fluka and Merck.

2.2 Electrode characterization

The surface morphology of the as-prepared cathode was analyzed by SEM (Hitachi S-4800). The XRD patterns were recorded on a BRUKER S5000 diffractometer, using Cu-Kα radiation (0.15418 nm) at 40 kV and 20 mA. FTIR Spectra of the powder LDH was performed on NEXUS FTIR (ThermoFisher). Surface chemistry of the LDH was studied by XPS (ESCALAB 250 Thermal Electron) using Al*Kα* (1486.6 eV). EIS (μ3AUT70466 Autolab System) was used to measure the interfacial-charge transfer resistance of the prepared cathodes. The EIS was carried out in an open circuit voltage with voltage amplitude of 10 mV in the frequency range from 50 kHz to 100 MHz.

2.3 EF experiment

The EF experiments were performed in an open, undivided cylindrical glass cell of diameter 4 cm and 150 mL capacity equipped with 24 cm^2 thin film Ti_4O_7 anode (Saint Gobain C.R.E.E., France), placed in parallel to the cathode (4.5 cm × 1 cm × 1.27 cm) made of either $Fe^{II}Fe^{III}$ or $Co^{II}Fe^{III}$ LDH/CF at a distance of approximately 2 cm. All experiments with the LDH/CF cathode were performed with 145 mL SMT solutions (0.2 mM) containing 0.05 M Na_2SO_4 as supporting electrolyte. The solution was constantly stirred with a PTFE magnetic bar to ensure mass transfer towards the electrodes. Compressed air was continuously bubbled into the solution at about 1 L min^{-1}, starting at 10 min prior to electrolysis to maintain a stationary O_2 concentration level. For comparison, analogous experiments were performed with raw carbon-felt cathode of similar size with the addition of 0.2 mM Fe^{2+} or without addition of any catalyst (EO-H_2O_2).

2.4 Instrument and analytic procedure

All electrolysis experiments were performed with a Hameg HM7042-5 triple power supply at constant current density of 7.5 mA cm^{-2}. The SMT solution pH was adjusted with 1 M H_2SO_4 or NaOH and was measured with a CyberScan pH 1500 pH-meter from Eutech Instruments. The mineralization of the SMT solutions was assessed from the decay of dissolved

organic carbon, which can be considered as the total organic carbon (TOC) for highly water soluble organic compounds. The TOC of initial and electrolyzed samples were measured on a Shimadzu TOC-L CSH/CSN analyzer. Reproducible TOC values with ± 2% accuracy were obtained using the non-purgeable organic carbon method. Calibration curves for total organic (TC) and inorganic carbon (IC) analysis were built up by automatic dilution of standards solutions containing potassium hydrogen phthalate and sodium hydrogen carbonate for TOC and IC, respectively. Percentage of TOC removal was calculated from to the following equation:

$$\text{TOC removal (\%)} = \frac{\Delta(\text{TOC})_{\text{exp}}}{\text{TOC}_0} \text{ x } 100 \qquad \text{(eq. 5)}$$

where $\Delta(\text{TOC})_{\text{exp}}$ is the experimental TOC decay at electrolysis time t (mg L^{-1}) and TOC_o is the corresponding initial value prior to electrolysis (in same unity).

The decay kinetics of SMT was followed by injecting 20 µL samples to the reversed-phase high performance liquid chromatography (HPLC) (Dionex) equipped with P680 HPLC pump and fitted with a Purosher RP-18, 5µm, 25 cm × 4.6 mm (i.d.) column at 40 ^{o}C. Detection was done with a UVD340U photodiode array detector selected at λ = 270 nm. Isocratic solvent mixture of methanol/water (containing 1% H_3PO_4) 25:75 (v/v) was used as mobile phase at a flow rate of 0.8 mL min^{-1}. The quantity of Fe^{2+} and total Fe leached into the treated solution from as-prepared $Fe^{II}Fe^{III}$ LDH/CF cathode at the pH 3, 6 and 9 was estimated by colorimetric technique in accordance with recipe reported elsewhere [37].

Short-chain carboxylic acids generated during the HEF treatment at pH 3 with $Fe^{II}Fe^{III}$ LDH/CF cathode were identified and quantified by ion-exclusion HPLC using Merck Lachrom liquid chromatograph equipped with a L-2130 pump fitted with a C18 Acclaim OA, 4 mm × 25 cm (i.d.) column at 40 ^{o}C, and coupled with a L-2400 UV detector selected at wavelength of 210 nm, using 1% H_2SO_4 at 0.2 mL min^{-1} as mobile phase. Aromatic intermediates formed after 30 min of HEF treatment of 0.5 mM SMT solutions at pH 3 were identified by GC-MS. The analyses were performed on a Trace 1300 gas chromatograph (Thermo scientific) coupled to a Single Quadrupole ISQ mass spectrophotometer according to method reported elsewhere [38]. The evolution of toxicity of the treated solution was studied by measuring the inhibition of the bio-luminescence of the bacteria *Allivibrio fischeri* formerly known as *Vibrio fischeri* using

Microtox® method. The pH of all the samples and blank was adjusted to 6.5 – 7.5 with the aid of 0.01 – 0.1 mM NaOH solution prior to Microtox analysis as described elsewhere [39].

3. Results and discussions

3.1 Electrode characterization

The $Fe^{II}Fe^{III}$ and $Co^{II}Fe^{III}$ LDH modified CF electrodes were prepared by *in-situ* solvothermal synthesis [40–42] using urea and ammonium fluoride as precipitation agent. Multiwall of either $Fe^{II}Fe^{III}$ or $Co^{II}Fe^{III}$ LDH were grown on CF at 100 ^{o}C using growth solutions containing either Fe^{2+} and Fe^{3+} or Co^{2+} and Fe^{3+} in urea and ammonium fluoride. During the hydrothermal treatment, there is gradual decomposition of $CO(NH_2)_2$ (eq. 6) and hydrolysis of NH_4F (eq. 7) which progressively increases the pH of the solution towards basic pH, thus induced simultaneous nucleation, crystallization and growth of the metallic hydroxides on the CF substrate [13]. The reactions at the hydrothermal temperature are given in eq. 6 – 8:

$$CO(NH_2)_{2(aq)} + 3H_2O_{(l)} + \Delta heat \rightarrow 2NH_4^{+}{}_{(aq)} + 2OH^{-}{}_{(aq)} + CO_{2(g)} \quad (6)$$

$$NH_4F_{(aq)} + H_2O_{(l)} \rightarrow NH_4^{+}{}_{(aq)} + OH^{-}{}_{(aq)} + HF_{(aq)} \quad (7)$$

$$Fe^{2+}/Co^{2+}{}_{(aq)} + Fe^{3+}{}_{(aq)} + OH^{-}{}_{(aq)} \rightarrow Fe^{II}Fe^{III}\ LDH/Co^{II}Fe^{III}\ LDH_{(s)} \quad 8)$$

The nucleation and growth of the LDH occurs majorly at the surface and within the CF immersed in the growth solution and the wall of the Teflon because both are high energy sites compared to the bulk of the solution [13].

The morphology of the raw and prepared modified cathode analyzed by SEM is shown in Fig. 1. The pretreated raw carbon-felt was cleaned and free from dirt as shown in Fig. 1a and 1b. After solvothermal treatment in Fe^{2+} and Fe^{3+} growth solution, extensive growth of dense platelets of $Fe^{II}Fe^{III}$ LDH covered each strands of the CF (Fig. 1c). A magnified image of Fig. 1c shows a rough, uneven and porous structure with some secondary phase precipitated along with the $Fe^{II}Fe^{III}$ LDH (Fig. 1d). Similar dense but hairy structures were grown on the CF when Co^{2+} and Fe^{3+} growth solution was utilized (Fig. 1e). The further magnification showed porous and

interconnected urchin-like structures which can enhance the diffusion of substance within the cathode [43].

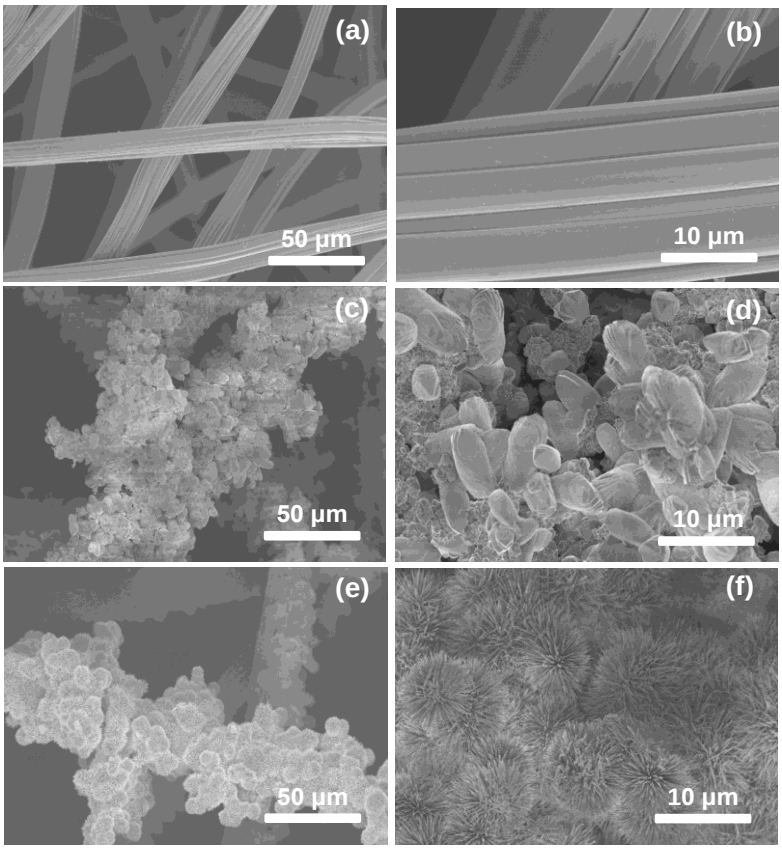

Figure 1: SEM images of (a,b) pretreated raw CF, (c,d) $Fe^{II}Fe^{III}$ LDH/CF and (e,f) $Co^{II}Fe^{III}$ LDH/CF.

Crystallinity of the prepared LDH modified CF as well as LDH powder were examined by XRD and showed in Fig. 2a and 2b. For both $Fe^{II}Fe^{III}$ and $Co^{II}Fe^{III}$ LDH modified CF, the XRD patterns of the powders and the modified CF indicated characteristics reflections corresponding to crystal planes of a typical hydrotalcite-like phase [44]. The diffraction peaks (2θ = 6^o, 12^o, 18^o, 23^o and 33^o) in Fig. 2a represent a layered structure with extensive growth of the crystal as depicted by the diffraction peaks between 2θ of 30^o and 55^o. Similar diffraction peaks (2θ = 12^o, 18^o, 23^o and 33^o) were observed with $Co^{II}Fe^{III}$ LDH (Fig 2b) along with some diffraction peaks between 30^o and 55^o also showed extensive growth of the LDH crystal. Both $Fe^{II}Fe^{III}$ and $Co^{II}Fe^{III}$ LDH crystal showed a good symmetry as depicted by couple of peaks at 57^o and 59^o 2θ (Fig. 2a and 2b). Additionally, the presence of some secondary phases in $Fe^{II}Fe^{III}$

LDH was shown by the diffraction peaks at 22^o, 31^o, 36^o and 62^o 2θ, corresponding to $Fe(OH)_3$, Fe_2O_3, maghemite Fe_2O_3 and transformation between $Fe(OH)_3$ and Fe_2O_3 respectively [44,45]. In contrast, no diffraction peaks of secondary phases were observed for $Co^{II}Fe^{III}$ LDH, which is in agreement with the SEM images (Fig. 1e and 1f). The peaks around 23^o and 43^o in lower diffractogram of both Fig. 2a and 2b are characteristic of the carbon substrate on which the LDH was deposited. It important to note that the intensity of the reflection peaks was significantly low with LDH modified CF compared to that of LDH powder.

The FTIR spectrum of the prepared $Fe^{II}Fe^{III}$ LDH powder measured in the wavelength range of 450 – 4000 cm^{-1} (Fig. 2c) showed two narrow bands at 3750 cm^{-1} and 3700 cm^{-1} assigned to stretching vibration of non-hydrogen and hydrogen bond O–H groups in the brucite sheet and interlayer of the $Fe^{II}Fe^{III}$ LDH. The peak located at 1650 cm^{-1} was associated with the bending vibration of absorbed water molecule onto the $Fe^{II}Fe^{III}$ LDH by hydrogen bonding. An intense peak at 1379 cm^{-1} was due to the N–O stretching mode of the surface adsorbed nitrate counter anions, which were incorporated from primarily $Fe(NO_3)_3.9H_2O$ of growth solution [43]. Besides, the bands in the low wavelength region of 580 – 800 cm^{-1} could be ascribed to stretching vibration of M–OH and M–O bondings (M = Fe) in the LDH [46]. Similar absorption bands were observed with $Co^{II}Fe^{III}$ LDH spectrum (inset panel of Fig. 2c) with peaks at 3690 cm^{-1}, 3470 cm^{-1}, 1610 cm^{-1} and 1420 cm^{-1} assigned to stretching vibration of non-hydrogen bond O–H, hydrogen bond O–H, bending vibration of absorbed water and N–O stretching mode of the interlayer nitrate respectively [43]. Further, the stretching vibration of M–OH and M–O bondings (M = Co and Fe) in the $Co^{II}Fe^{III}$ LDH could be observed between 540 – 800 cm^{-1}.

253

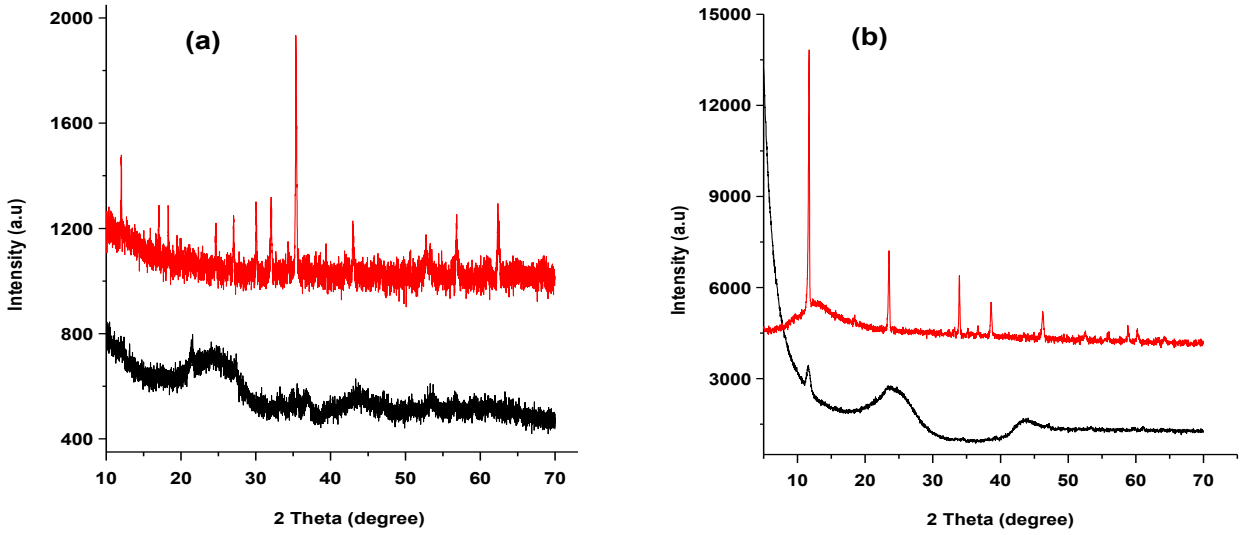
(a)
Intensity (a.u)
2 Theta (degree)
(b)
Intensity (a.u)
2 Theta (degree)

254

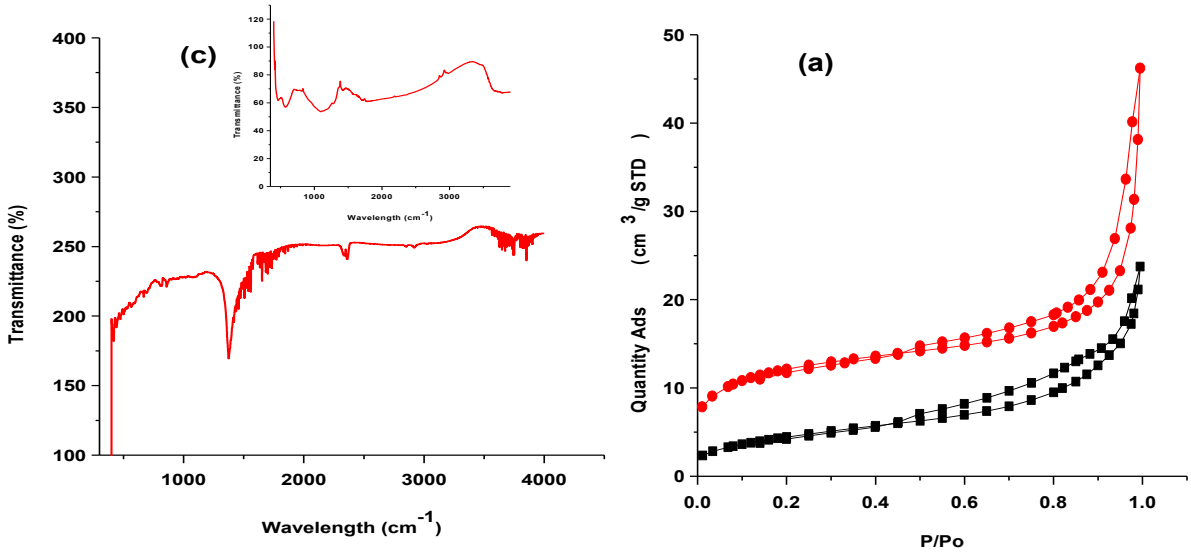
(c)
Transmittance (%)
Wavelength (cm-1)
(a)
Quantity Ads (cm 3/g STD)
P/Po

255

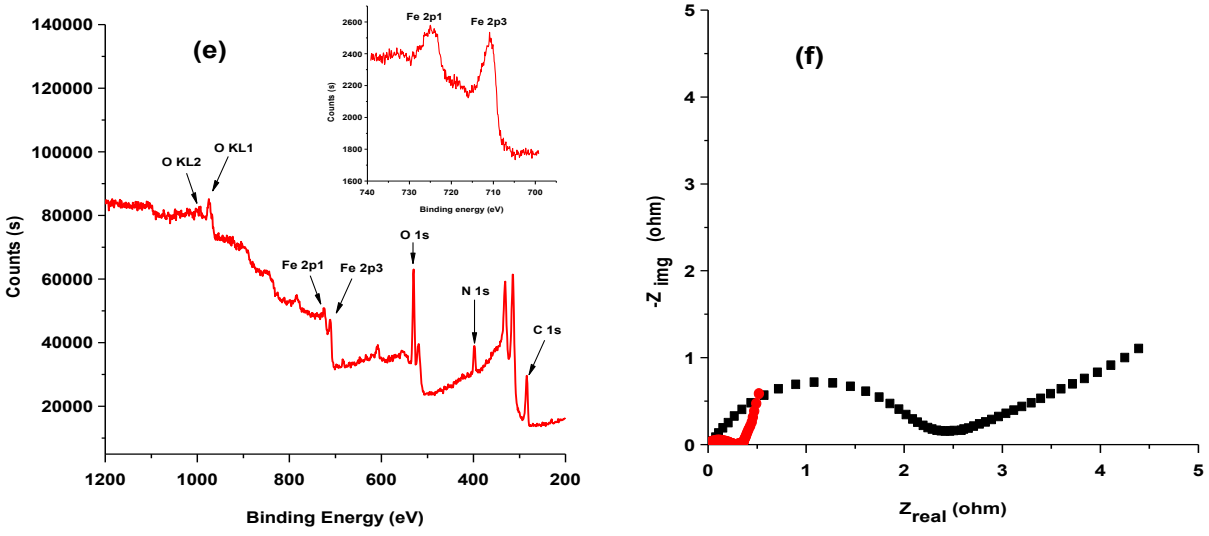
(e)
O KL2
O KL1
Fe 2p1
Fe 2p3
O 1s
N 1s
C 1s
Counts (s)
Binding Energy (eV)
(f)
-Z img (ohm)
Z real (ohm)

Figure 2: X-ray diffraction patterns of (a) $Fe^{II}Fe^{III}$ LDH powder (upper diffractogram) and $Fe^{II}Fe^{III}$ LDH/CF (lower diffractogram), (b) $Co^{II}Fe^{III}$ LDH powder (upper diffractogram) and $Co^{II}Fe^{III}$ LDH/CF (lower diffractogram), (c) FTIR spectrum of $Fe^{II}Fe^{III}$ LDH powder (inset panel: FTIR spectrum of $Co^{II}Fe^{III}$ LDH powder), (d) N_2 adsorption isotherm of (■) $Fe^{II}Fe^{III}$ LDH powder and (●) $Co^{II}Fe^{III}$ LDH powder [13], (e) XPS spectra existential state of O, Fe, N, C in the $Fe^{II}Fe^{III}$ LDH/CF (inset panel – XPS spectrum of Fe 2p) and (f) EIS spectra of (■) raw CF and (●)$Fe^{II}Fe^{III}$ LDH/CF obtained at 10 mV and 50 kHz – 100 MHz.

The N_2 adsorption isotherm for both LDH powder were shown in Fig. 2d, exhibiting type IV isotherm with a hysteresis loop typical of mesoporous material and regular pores as demonstrated by the adsorption-desorption plot. Additionally, the BET surface area of the $Fe^{II}Fe^{III}$ LDH powder was 16. 5 m^2 g^{-1} which was far less than 42.9 m^2 g^{-1} observed for $Co^{II}Fe^{III}$ LDH. The XPS spectra of the $Fe^{II}Fe^{III}$ LDH/CF are shown in Fig. 2e. The survey showed the existential state of elements like oxygen (KL and 1s), Fe (2p1 and 2p3), N (1s) as well as C (1s) indicating successful modification of CF. More so, the Fe 2p core lines split into 2p1 (725 eV) and 2p3 (711 eV) peaks with the former accompanied by a satellite band at around 732 eV (inset panel) [13].

The interface properties and potential of electron transfer between the electroactive substances and the prepared $Fe^{II}Fe^{III}$ LDH modified CF as well as raw CF was examined by EIS and presented in Fig. 2f. The interfacial charge-transfer resistance (Rc_t) was presented as suppressed semicircle arcs by the Nyquist plots with the diameter of the semicircle represent the actual value of the Rc_t. It is obvious from Fig. 2f that there was tremendous decrease in the interfacial resistance after the deposition of the $Fe^{II}Fe^{III}$ LDH, indicating significant enhancement in electron transfer. This could enhance the activity of the prepared cathode in terms of H_2O_2 production as well as Fe^{II}/Fe^{III} or Fe^{2+}/Fe^{3+} redox regeneration [47].

3.2 Mineralization and degradation of SMT: Effect of pH and cathode

The catalytic activity of the as-prepared $Fe^{II}Fe^{III}$ and $Co^{II}Fe^{III}$ LDH modified CF cathodes for the efficient electrochemical wastewater treatment over a wide pH range (pH 3 – 9) was investigated by studying the degradation and mineralization of the antibiotic SMT as a model

pollutant. It is worthy to state that both LDH/CF as well as the pretreated raw CF showed limited or no adsorption of the SMT with less than 1% TOC abatement after 8 h in control experiment (0 mA cm^{-2}) applied current density. The mineralization of SMT was studied with zero catalyst addition (*i.e.* EO-H_2O_2) using pretreated raw CF as cathode and Ti_4O_7 anode at different pH values. As shown in Fig. 3a, moderate TOC removal efficiency was attained during EO-H_2O_2 at all pH studied, achieving 64%, 63% and 53% TOC removal at pH 3, 6 and 9 respectively after 8 h of electrolysis. The mineralization of SMT in this case was mainly by physisorbed $Ti_4O_7(^{\bullet}OH)$ generated at the surface of the Ti_4O_7 anode since no catalyst was added to the treated solutions, therefore no $^{\bullet}OH$ production in the bulk solution [38,48,49]. Upon addition of optimized catalytic quantity of iron (0.2 mM Fe^{2+}) [30,49] to the treated solutions (*i.e.* EF-Fe^{2+}), an enhanced mineralization of SMT solution was achieved with TOC removal efficiency of 77%, 69% and 58% achieved at pH 3, 6 and 9 respectively. This enhanced mineralization of SMT was expected because of the contribution of homogeneously generated $^{\bullet}OH$ from Fenton's reaction (eq. 1) between electrogenerated H_2O_2 produced at the cathode and catalytic Fe^{2+} added to the solution prior to treatment [50,51]. The TOC removal efficiency during classical EF treatment was significantly reduced with increase in pH majorly due to the precipitation of the Fe^{2+} as hydroxides. In fact, the treated solutions at pH 6 and 9 remained yellow throughout electrolysis time, indicating the continuous presence of iron hydroxides in the solution; and the mineralization attained at these pHs was majorly by $Ti_4O_7(^{\bullet}OH)$ generated at the surface of the anode.

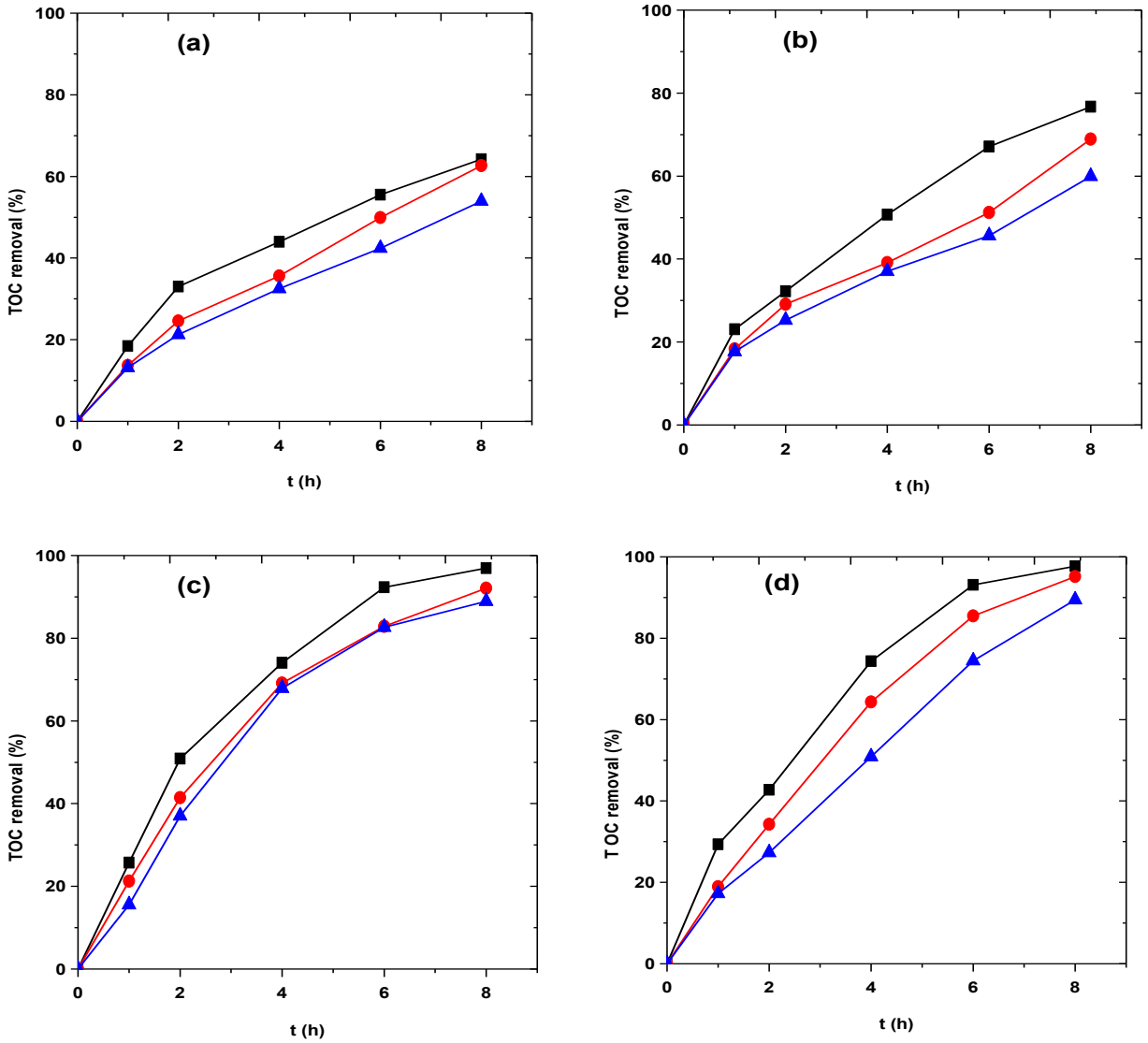

Figure 3: TOC removal efficiency *vs* time during the mineralization of 24 mg L^{-1} TOC SMT solution at: (■) pH 3, (●) pH 6 and (▲) pH 9 and current density of 7.5 mA cm^{-2} using (a) EO-H_2O_2, (b) EF-Fe^{2+}, (c) HEF with $Fe^{II}Fe^{III}$ LDH/CF and (d) Hetero-EF with $Co^{II}Fe^{III}$ LDH/CF cathodes (RSD: < 2%).

HEF with $Fe^{II}Fe^{III}$ LDH/CF cathode showed almost complete mineralization of SMT solutions over the pH range studied (Fig. 3c). In fact the initial pH of the treated solution has limited influence on the mineralization of SMT solutions during the HEF treatment. The excellent mineralization of SMT achieved with $Fe^{II}Fe^{III}$ LDH/CF at both acidic and basic pH can be attributed to surface catalyzed decomposition of H_2O_2 to produced $^{\bullet}OH$ which can easily oxidized SMT and its oxidation intermediates [12,17]. The surface catalyzed process widening

the pH window at which HEF can be carried out without necessarily reduced the efficiency of the process because the reaction occurs at solid-liquid interface in the treated solution. As shown in Figs. 3c and 4, less than 10% reduction in TOC removal efficiency was observed when the pH of the treated solution was increased from pH 3 to pH 9. Besides, the surface catalyzed process eliminates the formation of iron hydroxide sludge encountered in homogeneous EF since there was limited leaching of Fe from LDH at basic pH and the solution treated with LDH modified CF remained clear regardless of the initial solution pH. In comparison, HEF studies performed with $Co^{II}Fe^{III}$ LDH/CF showed almost similar mineralization efficiency with that obtained for $Fe^{II}Fe^{III}$ LDH/CF at all the studied pH values (Fig. 3d). For instance, the TOC removal efficiency of 97%, 93% and 90% was achieved at pH 3, 6 and 9 respectively with $Fe^{II}Fe^{III}$ LDH/CF (Fig. 4) which was approximately the same as 98%, 95% and 89% obtained with $Co^{II}Fe^{III}$ LDH/CF cathode at similar pH values, after 8 h of electrolysis. It is important to state that at acidic pH (*i.e.* pH 3), the oxidation of SMT was by both surface catalyzed process at the surface of the modified cathode and EF-Fe^{2+} oxidation arisen from the leaching of Fe^{2+}/Fe^{3+} and Co^{2+} from the LDH into the treated solution. The leached Fe^{2+}/Fe^{3+} and/or Co^{2+} can catalyzed the decomposition of H_2O_2 to produce $^{\bullet}OH$ in Fenton's reaction (eq. 1). The leaching of Fe and Co from the LDH and the quantity leached was confirmed and estimated by colorimetric method and detailed in section 3.3.

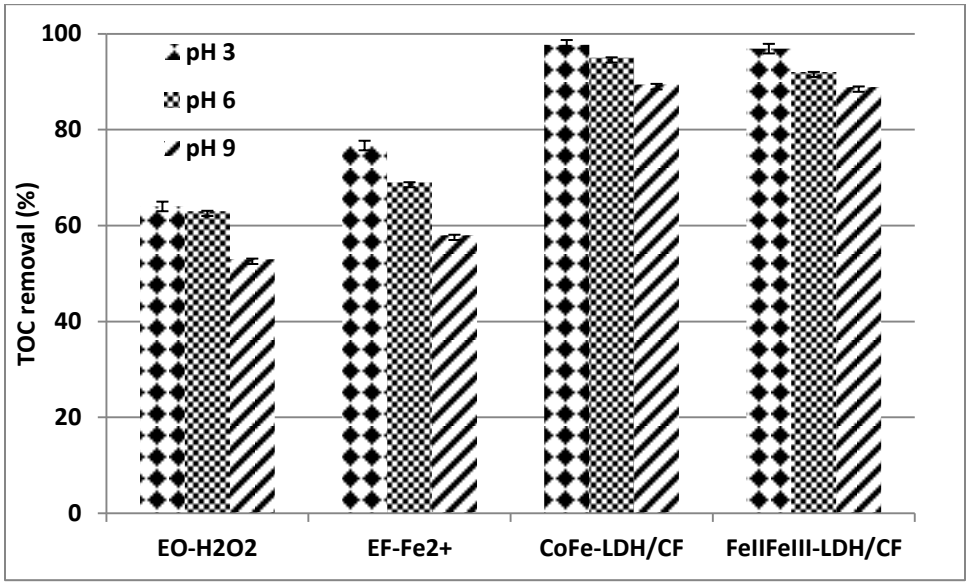

Figure 4: Comparison of the mineralization efficiency at different pHs for the treatment of 24 mg L^{-1} TOC SMT solution at current density of 7.5 mA cm^{-2} using EO-H_2O_2, EF-Fe^{2+}, HEF with $Co^{II}Fe^{III}$ LDH/CF and $Fe^{II}Fe^{III}$ LDH/CF.

Fig. 5 showed the corresponding SMT concentration decay with electrolysis time for all the trials of Fig. 3. Complete degradation of SMT was attained in all trials with time required for complete oxidation of SMT increases with pH for all the processes studied. As expected, much slower degradation was observed during EO-H_2O_2 (without Fe^{2+}) (Fig. 5a) compared to EF–Fe^{2+} or HEF because the Ti_4O_7($^{\bullet}$OH) are produced and confined to the anode region only, thus oxidation of SMT was mainly diffusion controlled [52]. At higher pH (pH 6 and 9) similar slower degradation was observed with EF-Fe^{2+}, which could be explained by the precipitation of the Fe^{2+} (catalyst) as ferric hydroxides from the solution, reducing the catalytic generation of $^{\bullet}$OH via Fenton's reaction. Indeed, both the degradation and mineralization of SMT solution at these pHs were performed predominantly by Ti_4O_7($^{\bullet}$OH) generated at the anode via water oxidation. Again, similar degradation efficiency was obtained during HEF process with both $Fe^{II}Fe^{III}$/CF and $Co^{II}Fe^{III}$ LDH/CF (Figs. 4c and 4d). For example, O.2 mM SMT was completely destroyed in treated solution after 40, 120 and 240 min at pH 3, 6 and 9 respectively with either $Fe^{II}Fe^{III}$/CF or $Co^{II}Fe^{III}$ LDH/CF cathode, demonstrating the efficiency of HEF for decontamination of SMT solutions.

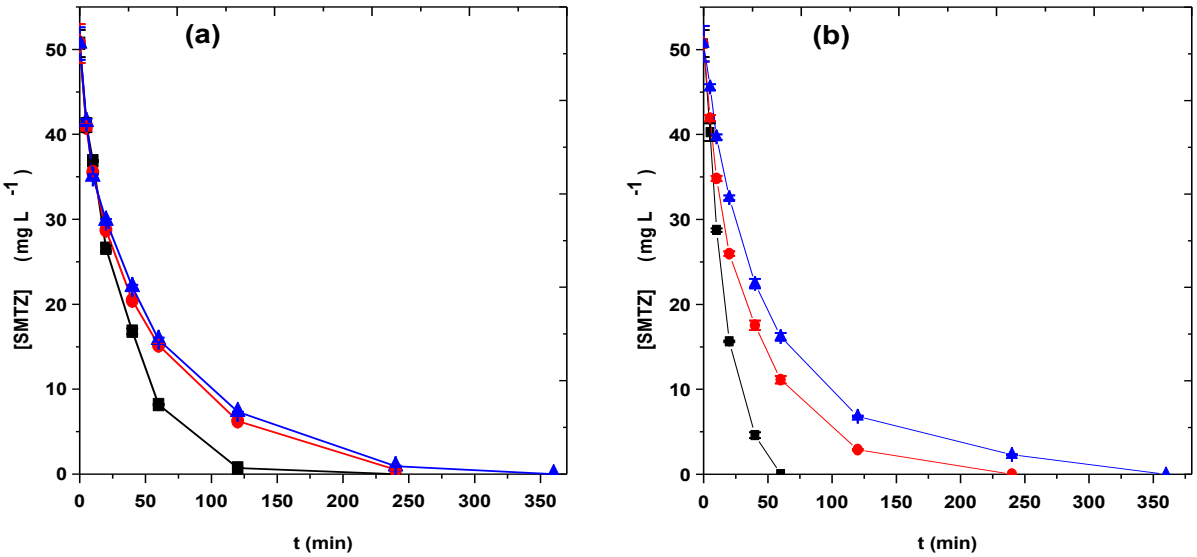

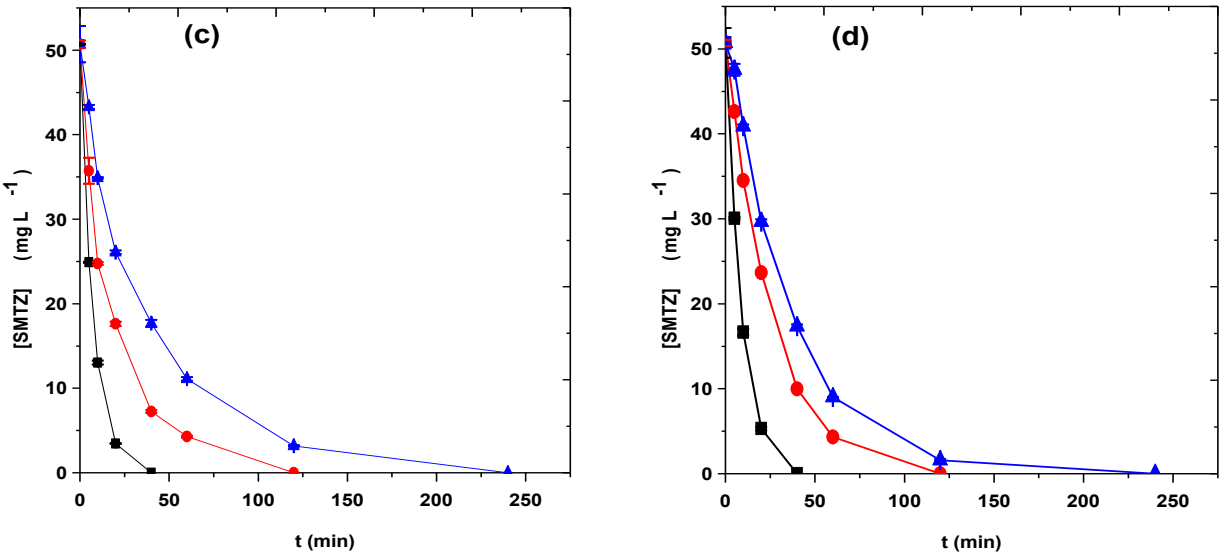

Figure 5: Concentration decay *vs* electrolysis time during the degradation of 50.7 mg L^{-1} (0.2 mM) SMT at: (■) pH 3 (●) pH 6 and (▲) pH 9 and current density of 7.5 mA cm^{-2} using (a) EO-H_2O_2, (b) EF- Fe^{2+}, (c) HEF with $Fe^{II}Fe^{III}$ LDH/CF and (d) HEF with $Co^{II}Fe^{III}$ LDH/CF.

3.3 Evolution of pH and Fe leaching during electrolysis

The initial pH of the wastewater and its evolution during electrochemical treatment based on Fenton's chemistry has a significant role on the efficiency of the process because the pH affects the availability of the Fe^{2+}/Fe^{3+} cycles (Fenton catalyst) in the solution. Indeed, Fe^{2+}/Fe^{3+} and other heavy metals precipitate as hydroxides as pH increases towards basic pH values. Additionally, the stability of both $Fe^{II}Fe^{III}$ and $Co^{II}Fe^{III}$ LDH used in HEF depend on the pH of the solution. In general, LDHs are less stable at strong acidic pH but barely affected at high pH [45] values. As such the evolution of pH of the SMT solution during treatment with $Fe^{II}Fe^{III}$ LDH/CF cathode was monitored and reported in Fig. 6a. There was sharp reduction in pH of the treated solution at the early stage of electrolysis when treated SMT solution at initial pH 9, but the solution pH remained almost unchanged after 1 h till the end of the treatment. Similar but gradual reduction in pH of the treated solution was observed at pH 6, but the pH kept nearly constant after 2 h of the treatment. The observed reduction in pH at the early stage of treatment can be attributed formation of short-chain carboxylic acids from the oxidative degradation of SMT and its cyclic byproducts [4–6]. In contrast, the pH of the treated solution was stable in

case of treated SMT solution at pH 3 (Fig. 6a), except for the early slightly increase observed within the first 10 min of electrolysis which was probably due to the inherited basic condition of preparing the cathode.

The quantities of Fe leached from the $Fe^{II}Fe^{III}$ LDH/CF cathode during the treatment of SMT solution at different initial pHs was reported in Fig. 6b. As depicted in Fig 6b, the prepared cathode showed very high stability at high initial SMT solution pH with the total Fe leached from the cathode less than 1 mg L^{-1} and 0.5 mg L^{-1} for the treatment at initial solution pH of 6 and 9, respectively. This implied that the contribution of homogeneous Fe^{2+}/Fe^{3+} catalyzed EF to the degradation of SMT solution was negligible and the mineralization of SMT was predominantly by surface catalyzed process at these pH values. However, the LDH became slightly unstable at strong acid pH (*i.e.* pH 3) and significant quantities of Fe (≈ 9 mg L^{-1}) were leached into the treated solution (Fig. 6b), suggesting the participation of EF-Fe^{2+} in the overall mineralization of the SMT solution at pH 3. The leached Fe existed in the solution as Fe^{2+}/Fe^{3+}, which can homogeneously catalyzed H_2O_2 decomposition to produce $^{\bullet}OH$. It is important to note that the Fe^{2+}/Fe^{3+} redox couple were continuously present in the solution, thanks to the formation of Fe^{3+} from Fenton's decomposition of H_2O_2 by Fe^{2+} (eq. 1) and cathodic reduction of Fe^{3+} to Fe^{2+} (eq. 3).

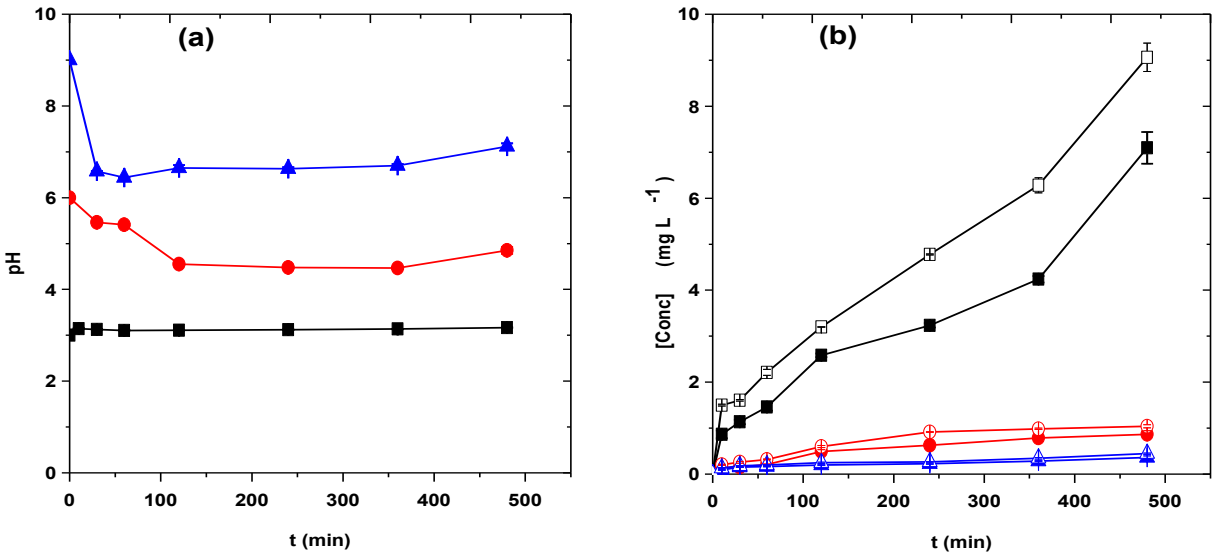

Figure 6: (a) Evolution of pH with electrolysis time: (■) pH 3, (●) pH 6 and (▲) pH 9; and (b) evolution of leached (■,●,▲) Fe^{2+} and (□,○,Δ) Fe_{Total} with electrolysis time at (■,□) pH 3, (●,○)

pH 6 and (▲,Δ) pH 9 during the treatment of SMT solution using $Fe^{II}Fe^{III}$ LDH/CF at current density of 7.5 mA cm^{-2}.

3.4 Evolution of oxidation by-products and reaction pathway

The mineralization of organic pollutants by hydroxyl radicals generated in electrochemical oxidation generally proceeds *via* the formation of several cyclic intermediates and release of heteroatoms as inorganic ions with the former further oxidized to short-chain carboxylic acids, which are the final end organic by-products in the treated solution [53]. The carboxylic acid generated during the HEF treatment of 0.2 mM SMT solution at pH 6 and current density of 7.5 mA cm^{-2} using $Fe^{II}Fe^{III}$ LDH/CF cathode was depicted in Fig. 7. Five distinctive peaks were shown on the HPLC chromatograms at 6.8, 8.2, 10.2, 14.3 and 16.4 min corresponding to oxalic, maleic, oxamic, glycoxylic and pyruvic acids. This was confirmed by injecting standard solutions of these acids into reversed phase HPLC using an ion-exclusion column. As shown in Fig. 7, accumulation – destruction cycle was observed for all the carboxylic acids, thanks to the rapid formation from oxidation of SMT and its cyclic intermediate at the early stage and mineralization of the acids with the increase in electrolysis time. Oxalic acid was the most accumulated as expected because it is the final end organic byproducts of oxidation of both cyclic and non-cyclic compound [54,55].

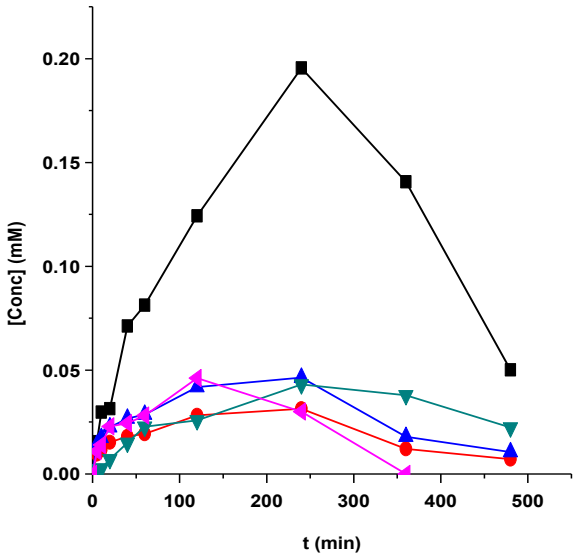

Figure 7: Time course of the main aliphatic carboxylic acids accumulated during HEF treatment of 0.2 mM SMT solution using $Fe^{II}Fe^{III}$ LDH/CF at pH 6 and current density of 7.5 mA cm^{-2}. Acids: (■) oxalic, (●) maleic (▲) oxamic, (▼) glycoxylic and (◀) pyruvic.

The GC-MS analysis of electrolyzed SMT solution after 60 min showed the formation of several aromatic/cyclic intermediates such as hydroxylated SMT (m/z = 267.9), 3-amino-5-methylisoxazole (m/z = 99.09), hydroxylated 3-amino-5-methylisoxazole (m/z = 116.18), 4-amino benzene sulfonamide (m/z = 175), hydroxylated 4-amino benzene sulfonamide (m/z = 191.6), hydroquinone and p-benzoquinone (m/z = 110). The 3-amino-5-methylisoxazole, hydroxylated SMT, hydroxylated 4-amino benzene sulfonamide, hydroquinone and p-benzoquinone have been identified as aromatic intermediate for SMT oxidation by other studies [30,31]. Based on these identified cyclic intermediates and the carboxylic acids, a proposed degradation pathway for complete mineralization of SMT by HEF using $Fe^{II}Fe^{III}$ LDH/CF cathode was given in Fig. 8, assuming hydroxyl radicals as the main oxidant. The degradation of SMT molecules was initiated either by the cleavage of the peptide bond to give 3-amino-5-methylisoxazole and 4-amino benzene sulfonamide or hydroxylation of SMT to hydroxylated SMT which can further undergoes cleavage of the peptide bond like original SMT molecule. Further hydroxylation, deamination and desulfonation of 4-amino benzene sulfonamide give p-benzoquinone which was further oxidized, along with deaminated 3-amino-5-methylisoxazole to several carboxylic acids that were finally mineralized to CO_2 and water.

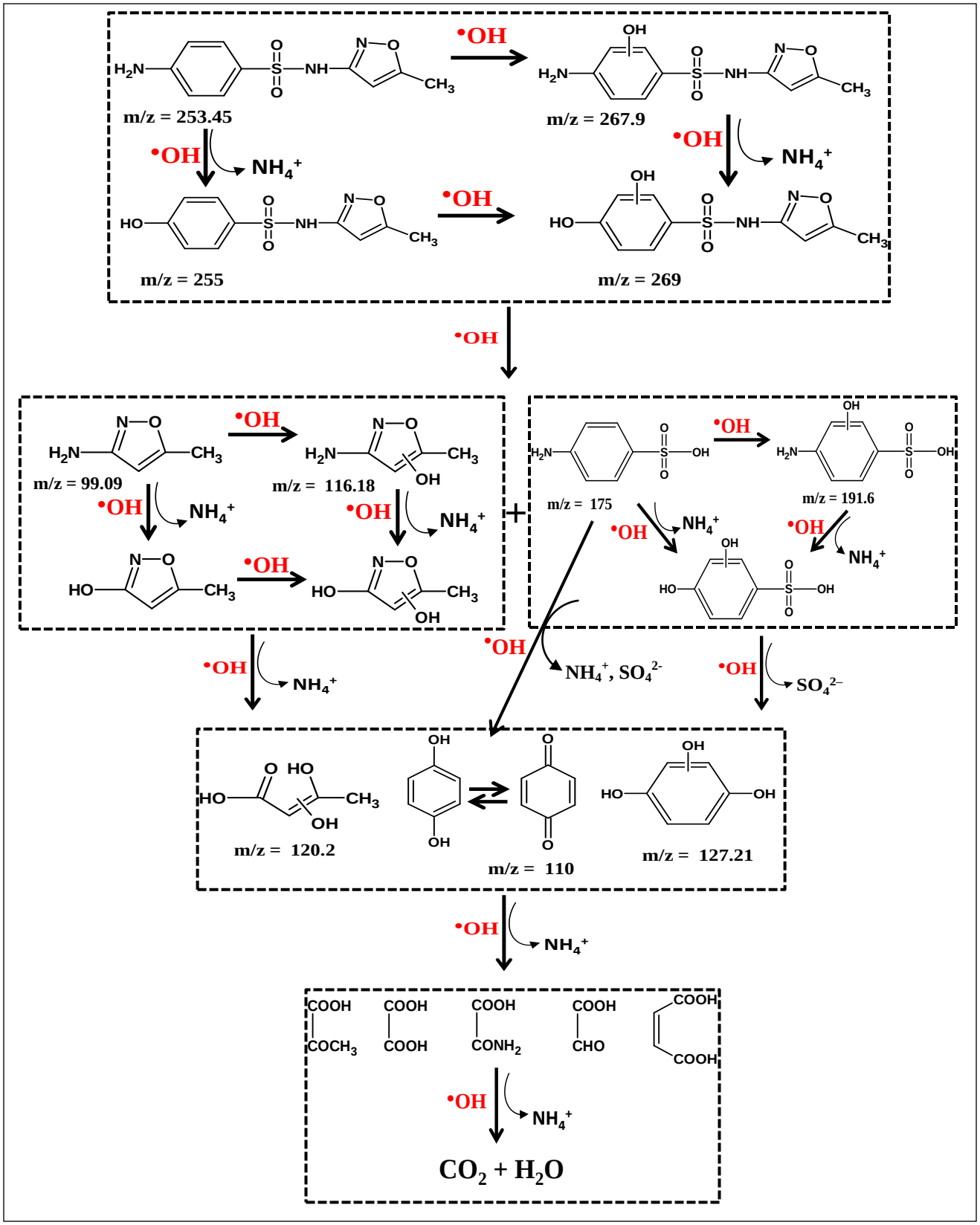
m/z = 253.45
m/z = 267.9
m/z = 255
m/z = 269
m/z = 99.09
m/z = 116.18
m/z = 175
m/z = 191.6
m/z = 120.2
m/z = 110
m/z = 127.21
•OH
NH4+
SO4 2–
NH4+, SO4 2-
CO2 + H2O

Figure 8: Reaction mechanism for complete degradation of SMT molecule assuming $^{\bullet}OH$ as main oxidant.

3.5 Assessment of toxicity and reusability of Fe(II)Fe(III)LDH/CF cathode

The evolution of toxicity of SMT solution with electrolysis time during the HEF treatment using $Fe^{II}Fe^{III}$ LDH/CF cathode at pH 3 and 6 was assessed by Microtox® method and reported in Figs. 9a and 9b. The initial SMT solution showed relatively high luminescence inhibition to *V. fischeri* bacteria at the beginning of electrolysis, demonstrating the toxicity of the antibiotic. The % luminescence inhibition sharply increased at the early stage of treatment owing to increased toxicity of the treated solution. Such sharp increase in bacteria inhibition can been attributed to the formation of aromatic/cyclic intermediates which are more toxic than the parent pollutant [30,50]. For treatment at pH 3, the high inhibition persisted up to 40 min of electrolysis before slight reduction and increment to second maximum, indicating the formation of secondary intermediates that are less toxic compared to primary cyclic byproducts. The % inhibition gradually reduced afterward until almost zero inhibition at the end of the treatment (Fig. 9a), demonstrating the total destruction of SMT, primary and secondary cyclic intermediates into biodegradable short-chain carboxylic acids and detoxification of the solution. Similar trend was observed for treatment at pH 6 (Fig. 9b), however the maximum inhibition of *V. fischeri* bacteria luminescence of treated solution at the early stage of electrolysis persisted for longer time (70 min) compared to what was observed at pH 3 (Fig. 9b), indicating slower degradation of aromatic intermediates at pH 6 in comparison with pH 3. This agrees well with the TOC removal efficiency reported in Fig. 3c.

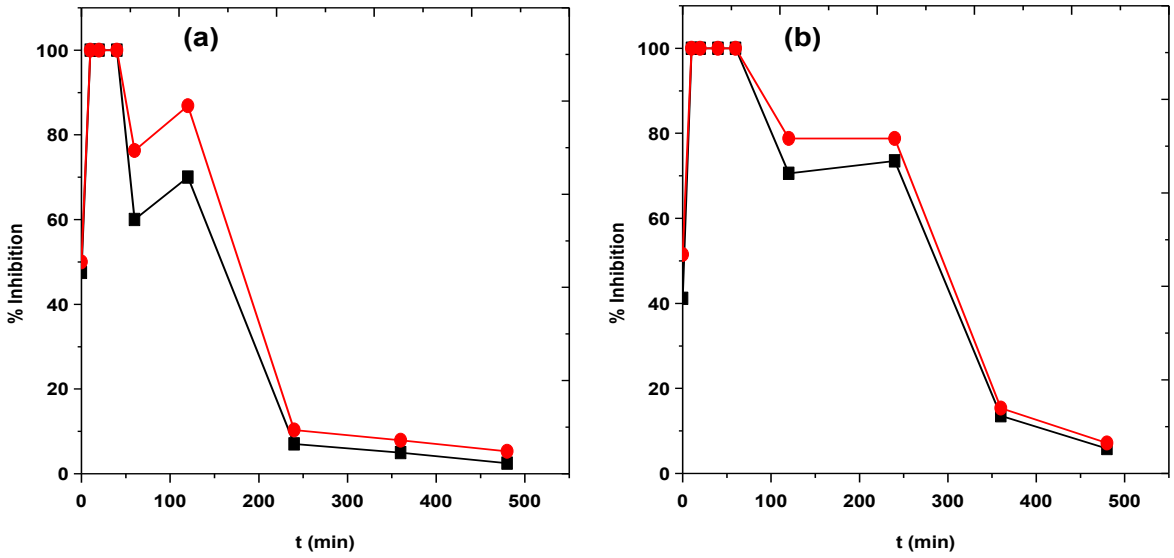

Figure 9: Evolution of % inhibition vs electrolysis time (a) pH 3 and (b) pH 6 after (■) 5 min and (●) 15 min of exposure to *V. fischeri* bacteria

The stability of the catalytic activity and reusability of the prepared $Fe^{II}Fe^{III}$ LDH/CF cathode for the mineralization and degradation of SMT solution at pH 6 was shown in Fig. 10. Excellent reusability over 10 cycles of 4 h treatment was observed for both mineralization and degradation of SMT solution. The catalytic efficiency of $Fe^{II}Fe^{III}$ LDH/CF showed less than 17% reduction in term of TOC removal efficiency over 10 cycles of 4 h treatment (Fig. 10a), demonstrating the efficacy of the HEF process for treatment of SMT solution. Interestingly, complete degradation of 0.2 mM SMT was always observed even after 10 cycles as depicted in Fig. 10b, indicating the high stability of the catalytic activity of the prepared cathode. Complete degradation of SMT was attained after 1 h of electrolysis for the first two cycles, whereas it requires over 2 h for the rest of the cycles, confirming the slight reduction in the catalytic activity of the cathode with reusability. As shown in Fig. 10a, the observed reduction in catalytic activity of the cathode over the 10 cycles was attributed to mechanical wearing of the LDH particles from the carbon-felt due to vigorous stirring, since the LDH is very stable at the working pH (pH 6) as reported in Fig. 6b.

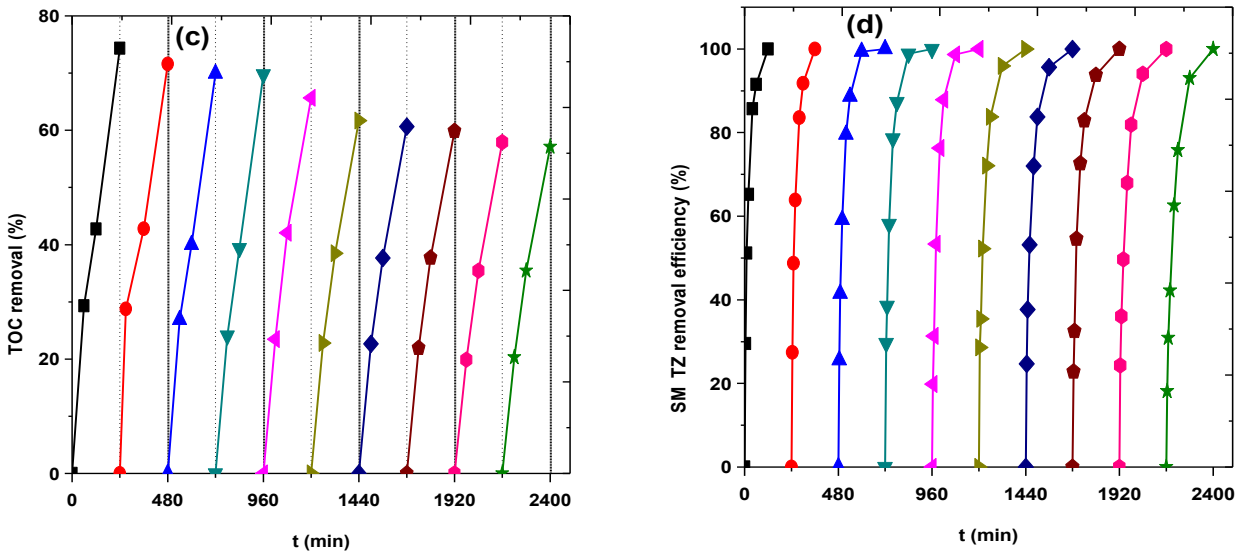

Figure 10: Reusability of $Fe^{II}Fe^{III}$ LDH/CF cathode at pH 6 with cycle (a) TOC removal and (b) SMT removal efficiency during the treatment of 0.2 mM SMT solution using $Fe^{II}Fe^{III}$ LDH/CF at 7.5 mA cm^{-2}.

3.6 Mechanism of mineralization of SMT at different pH

According to the previous studies [10,12], two different situations may be encountered depending on the pH of the treated solution and solubility of the solid Fe catalyst with pH. At low acidic pH (*i.e.* pH 3), the production of $^{\bullet}OH$ seems to be controlled by redox cycling of dissolved Fe^{2+}/Fe^{3+} resulting from the leaching of the LDH and surface Fe^{II}/Fe^{III} at the surface of the LDH. As such the mineralization and degradation of the SMT at pH 3 was a combined contribution of homogeneous and surface catalyzed (heterogeneous) processes, in addition to the oxidation by $Ti_4O_7(^{\bullet}OH)$ generated at the surface of the anode via water oxidation irrespective of pH. The *in-situ* H_2O_2 produced between the cathode and solution interface in acidic media is catalytically decomposed to stronger oxidizing agent $^{\bullet}OH$ by the surface bound $\equiv Fe^{II}/Fe^{III}$ or dissolved Fe^{2+}/Fe^{3+} in the bulk.

In contrast, at neutral and basic pH (pH 6 and 9), H_2O_2 decomposition was majorly by surface iron catalyzed process because LDH is almost insoluble at these pHs (Fig. 8b). HEF is a surface-catalyzed process controlled by many parameters such as H_2O_2 concentration, solution

pH and solid catalyst properties [12,17]. The kinetics and the reaction mechanism of the heterogeneous catalytic decomposition of H_2O_2 is not well-resolved in literature; however the formation of $^{\bullet}OH$ from catalytic decomposition of H_2O_2 by metal oxides is generally accepted as the most critical step in the entire oxidation process, which is similar to that of classical Fenton system as proposed by Harber-Weiss theory [12]. The $^{\bullet}OH$ formation in surface catalyzed process is initiated by interaction of H_2O_2 with the surface iron species like $\equiv Fe^{III}\text{—}OH$ and its one-electron reduced form, $\equiv Fe^{II}\text{—}OH$ (eq. 10), forming a surface complex of H_2O_2, $\equiv Fe^{III}\text{—}OH(H_2O_2)_s$ (eq. 11) at the inner and outer matrix of the carbon-felt [12,17]. The $\equiv Fe^{III}\text{—}OH(H_2O_2)_s$ complex may further undergo a reversible ground-state transfer (eq. 13) and activation (eq. 14) to form $\equiv Fe^{II}\text{—}OH$ and $HO_2^{\bullet}$. With the rapid consumption of H^+ in basic medium, the rate of eq. 13 and 14 can be significantly promoted, thus increasing the $^{\bullet}OH$ rate [17]. Beside, this could also explain the excellent mineralization of SMT observed at pH 6 and 9. Accordingly, the $\equiv Fe^{II}\text{—}OH$ catalyzes the decomposition of H_2O_2 to $^{\bullet}OH$ (eq. 15), which, along with $Ti_4O_7(^{\bullet}OH)$ can mineralize SMT and its intermediates to CO_2 and H_2O (eq. 16). Again in the case of $Co^{II}Fe^{III}$ LDH/CF, additional surface complex $Co^{II}\text{—}OH(H_2O_2)$ is formed, thus accelerate the production of $^{\bullet}OH$ [13]. The $^{\bullet}OH$ produced may either react directly with SMT molecules (eq. 15) or quenched by H_2O_2 (eq. 16) to form weak oxidant $HO_2^{\bullet}$. As such, high diffusion of the organic molecules (stirring) is necessary to ensure maximum reaction of $^{\bullet}OH$ with organic pollutant as well as minimize the scavenging of the $^{\bullet}OH$.

$$\equiv Fe^{III}\text{—}OH + e^- \rightarrow \equiv Fe^{II}\text{—}OH \quad (10)$$

$$\equiv Fe^{III}\text{—}OH + H_2O_2 \leftrightarrow \equiv Fe^{III}\text{—}OH(H_2O_2)_{(s)} \quad (11)$$

$$\equiv Fe^{III}\text{—}OH(H_2O_2)_{(s)} \rightarrow \equiv Fe^{II}\text{—}OH(HO_2^{\bullet})_{(s)} + H^+ \quad (12)$$

$$\equiv Fe^{II}\text{—}OH(HO_2^{\bullet})_{(s)} \rightarrow \equiv Fe^{II}\text{—}OH + HO_2^{\bullet} + H^+ \quad (13)$$

$$\equiv Fe^{II}\text{—}OH + H_2O_2 \rightarrow \equiv Fe^{III}\text{—}OH + {}^{\bullet}OH + OH^- \quad (14)$$

$$^{\bullet}OH/Ti_4O_7(^{\bullet}OH) + SMTZ \rightarrow CO_2 + H_2O \quad (15)$$

$$^{\bullet}OH + H_2O_2 \rightarrow HO_2^{\bullet} + H_2O \quad (16)$$

4. Conclusions

The oxidative degradation of the antibiotic SMT and mineralization of its aqueous solution at both acidic and basic medium by HEF system using $Fe^{II}Fe^{III}$ LDH/CF cathode was investigated. The $Fe^{II}Fe^{III}$ LDH was grown on CF by solvothermal process and the structural, chemical and electrochemical characterization reveals highly crystalline and porous structure containing FeOOH and Fe_2O_3 as secondary phase with enhanced conductivity. Excellent mineralization of SMT solutions was observed at all pHs studied with TOC removal of at least 90% attained after 8 h of treatment. Comparative studies with $Co^{II}Fe^{III}$ LDH/CF showed approximately the same mineralization and degradation efficiency at similar experimental conditions. In contrast, homogeneous EF optimized quantity of Fe^{2+} as well as EO-H_2O_2 using raw CF cathode showed poor mineralization of SMT solutions at all the studied pH in comparison to HEF with either $Fe^{II}Fe^{III}$ or $Co^{II}Fe^{III}$ LDH/CF cathode. The mineralization of SMT in HEF was by both Fe^{2+}/Fe^{3+} redox homogeneous catalyzed and surface catalyzed processes at strong acidic pH (pH 3), whereas surface catalyzed process was predominant at neutral or basic pH (pH 6 and 9) along with the contribution of TiO4(•OH) generated at the anode surface irrespective of pH. Catalytic activity of the prepared cathode was highly stable with negligible leaching at high pH and excellent reusability was achieved over 10 cycles of 4 h treatment. The initial SMT solution showed relatively high inhibition to *V. fischeri* bacteria but was totally detoxified to approximately zero percent inhibition after 8 h of treatment using $Fe^{II}Fe^{III}$ LDH/CF at pH 3 as well as pH 6. SMT degradation was *via* the formation of several cyclic intermediates which were later mineralized to short-chain carboxylic acids as the final end organic byproducts in the treated solution. Finally, based on identified intermediate products, a plausible mineralization pathway is proposed.

ACKNOWLEDGEMENTs The authors thank the EU for providing financial support through the Erasmus Mundus Joint Doctorate Programme ETeCoS^3 (Environmental Technologies for Contaminated Solids, Soils and Sediments, grant agreement FPA n°2010-0009) and the ANR

(French National Research Agency) funding through ANR ECO TS – CELectrON, (grant n°: ANR-13-ECOT-0003).

References

[1] M. Panizza, G. Cerisola, Direct and mediated anodic oxidation of organic pollutants, Chem. Rev. 109 (2009) 6541–6569.

[2] E. Brillas, I. Sires, M.A. Oturan, Electro-Fenton process and related electrochemical technologies based on Fenton's reaction chemistry, Chem. Rev. 109 (2009) 6570–6631.

[3] C.A. Martínez-Huitle, M.A. Rodrigo, I. Sirés, O. Scialdone, Single and coupled electrochemical processes and reactors for the abatement of organic water pollutants: A critical review, Chem. Rev. 115 (2015) 13362–13407.

[4] M.A. Oturan, J.J. Aaron, Advanced oxidation processes in water/wastewater treatment: Principles and applications. A review, Crit. Rev. Environ. Sci. Technol. 44 (2014) 2577–2641.

[5] M.A. Oturan, Electrochemical advanced oxidation technologies for removal of organic pollutants from water, Environ. Sci. Pollut. Res. 21 (2014) 8333–8335.

[6] M.A. Rodrigo, N. Oturan, M.A. Oturan, Electrochemically assisted remediation of pesticides in soils and water: A review, Chem. Rev. 114 (2014) 8720–8745.

[7] I. Sirés, E. Brillas, M.A. Oturan, M.A. Rodrigo, M. Panizza, Electrochemical advanced oxidation processes: today and tomorrow. A review, Environ. Sci. Pollut. Res. 21 (2014) 8336–8367.

[8] S.O. Ganiyu, E.D. van Hullebusch, M. Cretin, G. Esposito, M.A. Oturan, Coupling of membrane filtration and advanced oxidation processes for removal of pharmaceutical residues: A critical review, Sep. Purif. Technol. 156 (2015) 891–914.

[9] I. Sirés, E. Brillas, Remediation of water pollution caused by pharmaceutical residues based on electrochemical separation and degradation technologies: A review, Environ. Int. 40 (2012) 212–229.

[10] J. Li, Z. Ai, L. Zhang, Design of a neutral electro-Fenton system with Fe@Fe_2O_3/ACF composite cathode for wastewater treatment, J. Hazard. Mater. 164 (2009) 18–25.

[11] N. Qiao, H. Ma, M. Hu, Design of a neutral three-dimensional electro-Fenton system with various bentonite-based Fe particle electrodes: A comparative study, Mater. Res. Innov. 19 (2015) S2-137-S2-141.

[12] Y. Wang, G. Zhao, S. Chai, H. Zhao, Y. Wang, Three-Dimensional Homogeneous ferrite-carbon aerogel: One pot fabrication and enhanced electro-Fenton reactivity, ACS Appl. Mater. Interfaces. 5 (2013) 842–852.

[13] S.O. Ganiyu, T.X. Huong Le, M. Bechelany, G. Esposito, E.D. van Hullebusch, M.A. Oturan, M. Cretin, A hierarchical CoFe-layered double hydroxide modified carbon-felt cathode for heterogeneous electro-Fenton process, J Mater Chem A. 5 (2017) 3655–3666.

[14] A. Özcan, A. Atılır Özcan, Y. Demirci, E. Şener, Preparation of Fe_2O_3 modified kaolin and application in heterogeneous electro-catalytic oxidation of enoxacin, Appl. Catal. B Environ. 200 (2017) 361–371.

[15] L. Labiadh, M.A. Oturan, M. Panizza, N.B. Hamadi, S. Ammar, Complete removal of AHPS synthetic dye from water using new electro-fenton oxidation catalyzed by natural pyrite as heterogeneous catalyst, J. Hazard. Mater. 297 (2015) 34–41. doi:10.1016/j.jhazmat.2015.04.062.

[16] N. Barhoumi, H. Olvera-Vargas, N. Oturan, D. Huguenot, A. Gadri, S. Ammar, E. Brillas, M.A. Oturan, Kinetics of oxidative degradation/mineralization pathways of the antibiotic tetracycline by the novel heterogeneous electro-Fenton process with solid catalyst chalcopyrite, Appl. Catal. B Environ. 209 (2017) 637–647.

[17] G. Zhang, Y. Zhou, F. Yang, FeOOH-Catalyzed Heterogeneous Electro-Fenton System upon Anthraquinone@Graphene Nanohybrid Cathode in a Divided Electrolytic Cell: Catholyte-Regulated Catalytic Oxidation Performance and Mechanism, J. Electrochem. Soc. 162 (2015) H357–H365.

[18] C.M. Sánchez-Sánchez, E. Expósito, J. Casado, V. Montiel, Goethite as a more effective iron dosage source for mineralization of organic pollutants by electro-Fenton process, Electrochem. Commun. 9 (2007) 19–24.

[19] W.R.P. Barros, J.R. Steter, M.R.V. Lanza, A.C. Tavares, Catalytic activity of $Fe_{3-x}Cu_xO_4$ ($0 \leq x \leq 0.25$) nanoparticles for the degradation of Amaranth food dye by heterogeneous electro-Fenton process, Appl. Catal. B Environ. 180 (2016) 434–441.

[20] O. Iglesias, M.A.F. de Dios, T. Tavares, M.A. Sanromán, M. Pazos, Heterogeneous electro-Fenton treatment: preparation, characterization and performance in groundwater pesticide removal, J. Ind. Eng. Chem. 27 (2015) 276–282.

[21] C. Zhang, M. Zhou, G. Ren, X. Yu, L. Ma, J. Yang, F. Yu, Heterogeneous electro-Fenton using modified iron–carbon as catalyst for 2,4-dichlorophenol degradation: Influence factors, mechanism and degradation pathway, Water Res. 70 (2015) 414–424.

[22] J. Ramírez, L.A. Godínez, M. Méndez, Y. Meas, F.J. Rodríguez, Heterogeneous photo-electro-Fenton process using different iron supporting materials, J. Appl. Electrochem. 40 (2010) 1729–1736.

[23] S.B. Hammouda, F. Fourcade, A. Assadi, I. Soutrel, N. adhoum, A. Amrane, L. Monser, Effective heterogeneous electro-Fenton process for the degradation of a malodorous compound, indole, using iron loaded alginate beads as a reusable catalyst, Appl. Catal. B Environ. 182 (2016) 47–58.

[24] L. Bounab, O. Iglesias, E. González-Romero, M. Pazos, M. Ángeles Sanromán, Effective heterogeneous electro-Fenton process of m-cresol with iron loaded actived carbon, RSC Adv. 5 (2015) 31049–31056.

[25] H. Zhao, Y. Chen, Q. Peng, Q. Wang, G. Zhao, Catalytic activity of MOF(2Fe/Co)/carbon aerogel for improving H2O2 and OH generation in solar photo–electro–Fenton process, Appl. Catal. B Environ. 203 (2017) 127–137.

[26] H. Zhao, L. Qian, X. Guan, D. Wu, G. Zhao, Continuous Bulk FeCuC aerogel with ultradispersed metal nanoparticles: An efficient 3D heterogeneous electro-Fenton cathode over a wide range of pH 3–9, Environ. Sci. Technol. 50 (2016) 5225–5233.

[27] W. Chen, X. Yang, J. Huang, Y. Zhu, Y. Zhou, Y. Yao, C. Li, Iron oxide containing graphene/carbon nanotube based carbon aerogel as an efficient E-Fenton cathode for the degradation of methyl blue, Electrochimica Acta. 200 (2016) 75–83.

[28] E.G. Garrido-Ramírez, M.L. Mora, J.F. Marco, M.S. Ureta-Zañartu, Characterization of nanostructured allophane clays and their use as support of iron species in a heterogeneous electro-Fenton system, Appl. Clay Sci. 86 (2013) 153–161.

[29] L. Liang, Y. An, M. Zhou, F. Yu, M. Liu, G. Ren, Novel rolling-made gas-diffusion electrode loading trace transition metal for efficient heterogeneous electro-Fenton-like, J. Environ. Chem. Eng. 4 (2016) 4400–4408.

[30] A. Dirany, I. Sirés, N. Oturan, M.A. Oturan, Electrochemical abatement of the antibiotic sulfamethoxazole from water, Chemosphere. 81 (2010) 594–602.

669 [31] Y. Huang, T. Zhou, X. Wu, J. Mao, Efficient sonoelectrochemical decomposition of
670 sulfamethoxazole adopting common Pt/graphite electrodes: The mechanism and favorable
671 pathways, Ultrason. Sonochem. 38 (2017) 735–743.
672 [32] T.A. Ternes, Occurrence of drugs in German sewage treatment plants and rivers1Dedicated
673 to Professor Dr. Klaus Haberer on the occasion of his 70th birthday.1, Water Res. 32 (1998)
674 3245–3260.
675 [33] H. Lin, J. Niu, J. Xu, Y. Li, Y. Pan, Electrochemical mineralization of sulfamethoxazole by
676 Ti/SnO_2-Sb/Ce-PbO_2 anode: Kinetics, reaction pathways, and energy cost evolution,
677 Electrochimica Acta. 97 (2013) 167–174.
678 [34] N. Oturan, S.O. Ganiyu, S. Raffy, M.A. Oturan, Sub-stoichiometric titanium oxide as a new
679 anode material for electro-Fenton process: Application to electrocatalytic destruction of
680 antibiotic amoxicillin, Appl. Catal. B Environ. 217 (2017) 214–223.
681 [35] S.O. Ganiyu, N. Oturan, S. Raffy, G. Esposito, E.D. van Hullebusch, M. Cretin, M.A.
682 Oturan, Use of Sub-stoichiometric Titanium Oxide as a Ceramic Electrode in Anodic
683 Oxidation and Electro-Fenton Degradation of the Beta-blocker Propranolol: Degradation
684 Kinetics and Mineralization Pathway, Electrochimica Acta. 242 (2017) 344–354.
685 [36] A.M. Zaky, B.P. Chaplin, Porous substoichiometric TiO_2 anodes as reactive
686 electrochemical membranes for water treatment, Environ. Sci. Technol. 47 (2013) 6554–
687 6563.
688 [37] M. Griffing, M.G. Mellon, Colorimetric determination of iron with various dioximes, Anal.
689 Chem. 19 (1947) 1017–1020.
690 [38] S.O. Ganiyu, N. Oturan, S. Raffy, M. Cretin, R. Esmilaire, E. van Hullebusch, G. Esposito,
691 M.A. Oturan, Sub-stoichiometric titanium oxide (Ti_4O_7) as a suitable ceramic anode for
692 electrooxidation of organic pollutants: A case study of kinetics, mineralization and toxicity
693 assessment of amoxicillin, Water Res. 106 (2016) 171–182.
694 [39] T.X.H. Le, T.V. Nguyen, Z.A. Yacouba, L. Zoungrana, F. Avril, D.L. Nguyen, E. Petit, J.
695 Mendret, V. Bonniol, M. Bechelany, S. Lacour, G. Lesage, M. Cretin, Correlation between
696 degradation pathway and toxicity of acetaminophen and its by-products by using the
697 electro-Fenton process in aqueous medium, Chemosphere 172 (2017) 1 – 9.

[40] X. Cai, X. Shen, L. Ma, Z. Ji, C. Xu, A. Yuan, Solvothermal synthesis of NiCo-layered double hydroxide nanosheets decorated on RGO sheets for high performance supercapacitor, Chem. Eng. J. 268 (2015) 251–259.

[41] Y. Han, Z.H. Liu, Z. Yang, Z. Wang, X. Tang, T. Wang, L. Fan, K. Ooi, Preparation of $Ni^{2+}Fe^{3+}$ Layered Double Hydroxide Material with High Crystallinity and Well-Defined Hexagonal Shapes, Chem. Mater. 20 (2008) 360–363.

[42] J. Zhao, J. Chen, S. Xu, M. Shao, D. Yan, M. Wei, D.G. Evans, X. Duan, CoMn-layer double hydroxide nanowalls supported on carbon fibers for high-performance flexible energy storage devices, J. Mater. Chem., 1 (2013) 8836–8843.

[43] G. Nagaraju, G.S.R. Raju, Y.H. Ko, J.S. Yu, Hierarchical Ni–Co layered double hydroxide nanosheets entrapped on conductive textile fibers: a cost-effective and flexible electrode for high-performance pseudocapacitors, Nanoscale. 8 (2016) 812–825.

[44] Q. Wang, S. Tian, J. Long, P. Ning, Use of Fe(II)Fe(III)-LDHs prepared by co-precipitation method in a heterogeneous-Fenton process for degradation of Methylene Blue, Catal. Today. 224 (2014) 41–48.

[45] X. Long, Z. Wang, S. Xiao, Y. An, S. Yang, Transition metal based layered double hydroxides tailored for energy conversion and storage, Mater. Today. 19 (2016) 213 - 226.

[46] Y. Li, L. Zhang, X. Xiang, D. Yan, F. Li, Engineering of ZnCo-layered double hydroxide nanowalls toward high-efficiency electrochemical water oxidation, J. Mater. Chem. A. 2 (2014) 13250.

[47] T.X. Huong Le, M. Bechelany, M. Cretin, Carbon felt based-electrodes for energy and environmental applications: A review, Carbon. 122 (2017) 564–591.

[48] P. Geng, J. Su, C. Miles, C. Comninellis, G. Chen, Highly-Ordered Magnéli Ti4O7 Nanotube Arrays as Effective Anodic Material for Electro-oxidation, Electrochimica Acta. 153 (2015) 316–324.

[49] D. Bejan, J.D. Malcolm, L. Morrison, N.J. Bunce, Mechanistic investigation of the conductive ceramic Ebonex® as an anode material, Electrochimica Acta. 54 (2009) 5548–5556.

[50] N. Oturan, J. Wu, H. Zhang, V.K. Sharma, M.A. Oturan, Electrocatalytic destruction of the antibiotic tetracycline in aqueous medium by electrochemical advanced oxidation processes: Effect of electrode materials, Appl. Catal. B Environ. 140–141 (2013) 92–97.

[51] A. Dirany, I. Sirés, N. Oturan, A. Özcan, M.A. Oturan, Electrochemical treatment of the antibiotic sulfachloropyridazine: Kinetics, reaction pathways, and toxicity Evolution, Environ. Sci. Technol. 46 (2012) 4074–4082.

[52] E. Brillas, S. Garcia-Segura, M. Skoumal, C. Arias, Electrochemical incineration of diclofenac in neutral aqueous medium by anodic oxidation using Pt and boron-doped diamond anodes, Chemosphere. 79 (2010) 605–612.

[53] A. Özcan, Y. Şahin, A.S. Koparal, M.A. Oturan, A comparative study on the efficiency of electro-Fenton process in the removal of propham from water, Appl. Catal. B Environ. 89 (2009) 620–626.

[54] M.A. Oturan, M. Pimentel, N. Oturan, I. Sirés, Reaction sequence for the mineralization of the short-chain carboxylic acids usually formed upon cleavage of aromatics during electrochemical Fenton treatment, Electrochimica Acta. 54 (2008) 173–182.

[55] S. Garcia-Segura, E. Brillas, Mineralization of the recalcitrant oxalic and oxamic acids by electrochemical advanced oxidation processes using a boron-doped diamond anode, Water Res. 45 (2011) 2975–2984.